pISSN 1229-845X, eISSN 1976-555X
J. Vet. Sci. (2011), **12**(2), 107-113
DOI: 10.4142/jvs.2011.12.2.107
Received: 24 Feb. 2010, Accepted: 10 Dec. 2010

JOURNAL OF
Veterinary Science

Original Article

Real time observation of mouse fetal skeleton using a high resolution X-ray synchrotron

Dong Woo Chang[1,2], Bora Kim[3,4], Jae Hoon Shin[5,7], Young Min Yun[9], Jung Ho Je[4], Yeu kuang Hwu[10], Jung Hee Yoon[6,7,8], Je Kyung Seong[5,7,8,*]

[1]Department of Radiology, College of Veterinary Medicine, Chungbuk National University, Cheongju 361-763, Korea
[2]Medical Research Center, College of Medicine, Yonsei University, Seoul 120-752, Korea
[3]Animal Science Branch, National Cancer Center, Koyang 410-769, Korea
[4]Department of Materials Sciences, Pohang University of Science and Technology, Pohang 790-784, Korea
Departments of [5]Anatomy and Cell Biology, and [6]Radiology, College of Veterinary Medicine, and [7]BK21 Program for Veterinary Science, and [8]Research Institute for Veterinary Science, Seoul National University, Seoul 151-742, Korea
[9]Department of Internal Medicine, College of Veterinary Medicine, Jeju National University, Jeju 690-756, Korea
[10]Institute of Physics, Academia Sinica, 128 Academic Rd., Nankang, Taipei 11529, Taiwan

The X-ray synchrotron is quite different from conventional radiation sources. This technique may expand the capabilities of conventional radiology and be applied in novel manners for special cases. To evaluate the usefulness of X-ray synchrotron radiation systems for real time observations, mouse fetal skeleton development was monitored with a high resolution X-ray synchrotron. A non-monochromatized X-ray synchrotron (white beam, 5C1 beamline) was employed to observe the skeleton of mice under anesthesia at embryonic day (E)12, E14, E15, and E18. At the same time, conventional radiography and mammography were used to compare with X-ray synchrotron. After synchrotron radiation, each mouse was sacrificed and stained with Alizarin red S and Alcian blue to observe bony structures. Synchrotron radiation enabled us to view the mouse fetal skeleton beginning at gestation. Synchrotron radiation systems facilitate real time observations of the fetal skeleton with greater accuracy and magnification compared to mammography and conventional radiography. Our results show that X-ray synchrotron systems can be used to observe the fine structures of internal organs at high magnification.

Keywords: mouse, real-time observation, X-ray synchrotron

Introduction

Although X-rays represent one of the most important diagnostic imaging methods for radiotherapy, they are associated with a number of limitations including insufficient spatial resolution, contrast, and quantitative scale [24]. Recently, computed tomography (CT) and magnetic resonance imaging (MRI) have been found to produce higher quality results along with more information on internal structures, and can be used as non-invasive screening tools. However, these techniques are unable to detect micro-sized fine structures for the early diagnosis of tumors, vascular diseases, and other disorders [10].

The advent of synchrotron radiation has added a new dimension to the use of X-rays for imaging and radiotherapy. Synchrotron radiation has the potential to provide new solutions to the problems associated with other imaging modalities such as CT and MRI [24]. Because of its high brilliance and laser beam-like directionality, synchrotron radiation can provide ultra-high resolution images using a small field of view. The use of synchrotron radiation sources may enable considerable improvements in some imaging techniques routinely used in medicine. Synchrotron radiation has been used for several different techniques, including venous coronary angiography, digitized cerebral synchrotron radiation angiography, monochromatic X-ray computed tomography, monochromatic mammography, two wavelength digital subtraction angiography, phase-contrast/edge-enhancement imaging, diffraction-enhanced imaging, and microtomography, in several countries including the United States, Germany, and Japan [9,11,13-15,19,25]. In addition, synchrotron-based K-edge digital subtraction angiography is another imaging technique that is highly sensitive to low concentrations of contrast agents. It has been recently reported that K-edge digital subtraction angiography is particularly useful for studying neurovascular pathology in pigs [21].

In teratologic studies, experiments investigating the effect

*Corresponding author
Tel: +82-2-880-1259; Fax: +82-2-875-8395
E-mail: snumouse@snu.ac.kr

of various teratogens (including carbon monoxide, X-rays, or ethanol exposure) on the developing embryo have found that these factors produce vertebral and other skeletal anomalies in the offspring of mice. These abnormalities of the fetus had been observed by fetal tissue double-staining using Alizarin red and Alcian blue, gross inspection, radiography, or mammography [2,3,16,17,22,23]. However, the mouse fetus is only about 18～20 mm in size from crown to rump, making it extremely difficult to use these modalities for observing small lesions.

In this study, we used synchrotron radiation to obtain a high definition X-ray image of the fetus *in utero*. The fetus removed from the ICR mouse and the time at which the fetal skeleton could be observed was estimated. Our results might be used to find new technologies that enable real-time observation of fine structures without staining.

Materials and Methods

Experimental animals

Pregnant ICR mice (body weight 43.1～72.7 g) were purchased from commercial breeders (Daehan Biolink, Korea) and fed a standard chow (LabDiet, USA). The first day of gestation was designated as the day after observing the vaginal plug. The Committee for the Care and Use of Laboratory Animals in Yonsei University (Korea) reviewed and approved the protocols for our study according to the Guidelines for Animal Experiments edited by the Korean Academy of Medical Sciences.

Imaging system and data acquisition

We examined the animals using a Min-R Screen-Film system (Eastman Kodak, USA) and conventional mammography equipment (Performa; GE Healthcare, USA) with 24 kVp, 60 mA and 0.5 sec of exposure time. The film was processed with and automatic processor (Model 2000; Kodak, USA). The experiments were carried out on a 5C1 beamline at the Pohang Accelerator Laboratory (Pohang University of Science and Technology, Korea) with a 2.5 GeV, 150 mA storage ring current, and 1.32 T magnetic field. The electric field was used with S type of polarization in the plane of ring. Since longitudinal coherence is not a stringent requirement for refractive index radiology, non-monochromatized ("white") light was used with no optical elements except beryllium windows. After the beam went through the window into air, we introduced slit and attenuator systems to minimize damage associated with the scintillator and to prevent background image over-saturation. The detection system was based on a $CdWO_4$ single crystal scintillator cleaved to a thickness of < 100 μm of silica which was resistant to radiation damage and highly homogeneous. The high-resolution radiograph on the scintillator was magnified with an optical lens, captured by a commercial-grade CCD video camera (IK-536; Toshiba, Japan), and recorded with a digital video recorder (GV-D300; Sony, Japan). To prevent oversaturation, an ND4 filter and 52S polarizer (Kenko, Japan) were used (Fig. 1). The background image obtained just before fetus imaging was stored as a digital image and a temporal subtraction image using a computer. After synchrotron radiation imaging, one mouse was randomly selected and euthanized on gestation day 18 and its fetuses were removed for synchrotron radiation analysis.

Experimental procedures

Mice were anesthetized with intraperitonial injections of ketamine (22.5 mg/kg; Yuhan, Korea) and xylazine (1.75 mg/kg; Bayer, Germany). Two mice at embryonic day (E)12, four mice at E14, two mice at E15, and two mice at E18 were radiographed with conventional X-ray (VPX-100A; Toshiba, Japan) and mammography equipment. To observe fetal anatomy, the pregnant mice were suspended around the rectangular positioner with surgical ties and placed in a vertical position (Fig. 2). The anesthetized mice were imaged with synchrotron radiation on the 5C1 beamline. Synchrotron radiation was derived from an accumulation ring of electrons with an accelerated energy of 2.5 Gev.

One mouse at E12, E14, E15, and E18 was anesthetized after synchrotron radiation imaging and the fetuses were removed. Each fetus was skinned and eviscerated for the bone and cartilage staining with Alizarin red S and Alcian blue. The fetal tissues were fixed in 95% ethanol for 48 h at room temperature. The staining solutions were composed of those two reagents and prepared as follows. The staining solution was mixed with 0.12% Alizarin red S in 95% ethanol and 0.14% Alcian blue in 75% ethanol. This solution was added into mixture of glacial acetic acid 10 mL and 70% ethanol 170 mL at room temperature for three days. Specimens

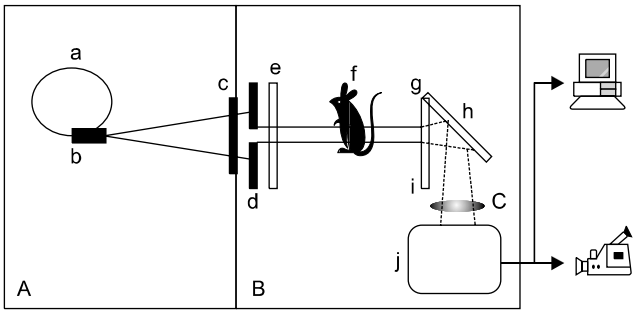

Fig. 1. Schematic diagram of the experimental set-up. Polychromatic X-rays (A), are emitted from the bending magnet device (b) of the storage ring (a) then pass through two slits (c: fixed one in the vacuum, d: changeable in the air) to control the beam size, attenuator set (e) for acquiring a good background image, and sample (f). The X-rays are processed by the scintillator (g) and the resulting image information is then converted into visible light (B). This visible light is magnified (C) by lens (i) after being reflected by the mirror (h) and transmitted to a computer or digital video recorder by the CCD camera (j).

Fig. 2. Photograph of a pregnant mouse suspended in the rectangular positioner with surgical ties. Synchrotron radiation imaging was performed with the mouse in an upright position.

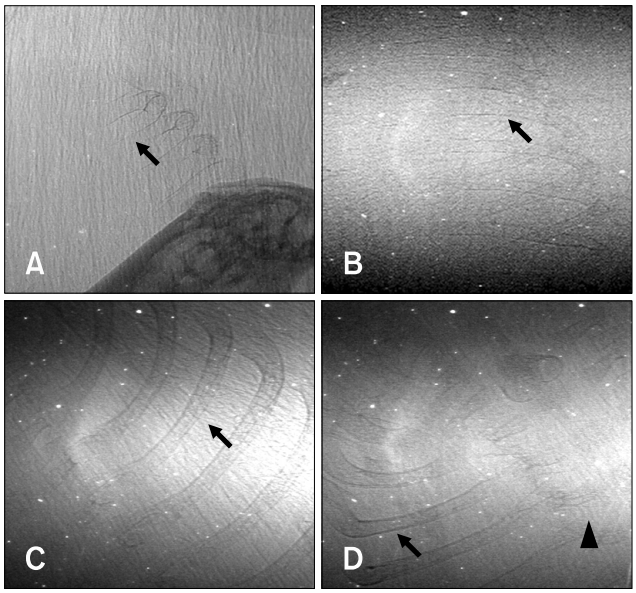

Fig. 3. Photographs of a mouse fetus thorax obtained by synchrotron radiation at embryonic day (E) 14 (A), E15 (B), and E18 (C, D). At E18, fetal ribs (arrows) and thoracic vertebra (arrowhead) were observed. Fetal ribs were also visualized at E14 and E15 but with lower definition.

were macerated in 1% KOH for two days at room temperature and then cleared through 1% KOH in 20% glycerol. The specimens were then stored in 100% glycerol and photographed using a stereomicroscope (Stemi V6; Zeiss, Germany).

Results

Ten fetuses were visualized at E12, E14, E15, and E18 after gestation using a synchrotron radiation system. Fetal bones were not visualized in two mice at E12. Fig. 3A shows representative fetal ribs at E14; some portions of the ribs could not be viewed because they overlapped the mother's femur. Fetal bones were visualized in three out of four mice examined at E14 using the synchrotron radiation system. As shown in Fig. 3B, fetal ribs could be better observed (radiopaque) compared to E12. However, other bony structures were not visualized at this period by the synchrotron radiation system. Figs. 3C and D show that fetal ribs were more apparent and adjacent thoracic vertebrae were identified at E18. At E15 and E18, fetal bony structures were visualized in all mice examined (Table 1).

Data use to identify fetal bony structures using synchrotron radiation, conventional radiography, and mammography equipment are shown in Table 2. In conventional radiography, fetal bony structures were first visualized in one mouse at E18. This method enabled visualization of the uterus containing several fetuses and radiodense fetal bony structures; however, it was difficult to specifically identify fetal anatomic structures because of low resolution (Fig. 5D). Fetal bony structures were first visualized with mammography equipment in one mouse at E15 and two mice at E18. As shown in Fig. 5C, fetal

Table 1. Data for the visualization of fetal skeleton in mouse using synchrotron radiation following the embryonic day

Animal No.	E12	E14	E15	E18	Identified structures
1	X				−
2	X				−
3		0			Ribs
4		0			Ribs
5		0			Ribs
6		X			−
7			0		Ribs
8			0		Ribs
9				0	Ribs, thoracic vertebra
10				0	Ribs, thoracic vertebra

0: observed, X: not observed, −: not specified.

Table 2. Visualization of fetal bony structures at embryonic day using synchrotron, mammography, and conventional radiography

Imaging modalities	E12	E14	E15	E18
Synchrotron	0/2	3/4	2/2	2/2
Mammography	0/2	0/3	1/2	2/2
Conventional radiography	0/2	0/2	0/2	1/2

Ratios indicate the number of mice in which bony structures were identified/number of mice examined.

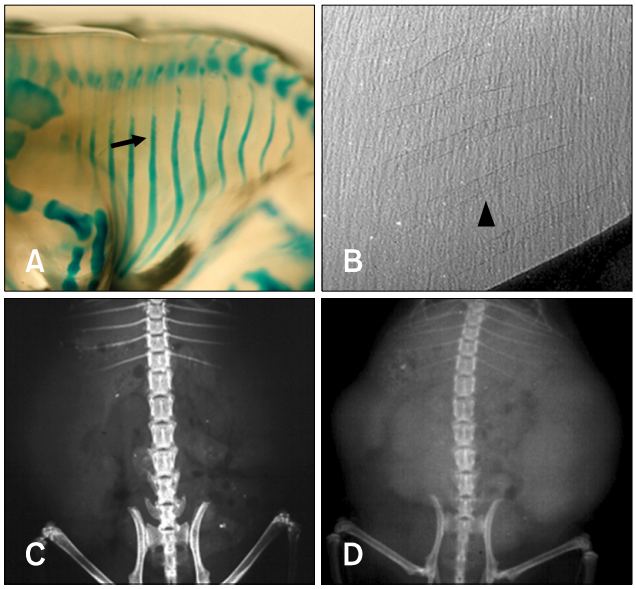

Fig. 4. Photographs of a fetus stained with Alizarin red S and Alcian blue (A) and images of fetal ribs obtained with synchrotron radiation (B), mammography (C), and conventional radiography (D) in a pregnant mouse at E14. Although the ribs had not yet calcified (arrow), they were visualized with synchrotron radiation (arrowhead). However, the ribs were not observed with the mammography equipment or conventional radiography.

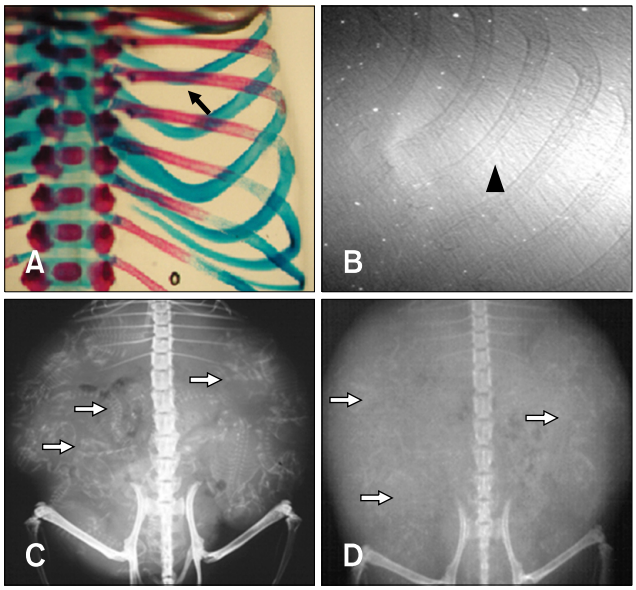

Fig. 5. Photographs of a fetus stained with Alizarin red S and Alcian blue (A) and images of fetal ribs obtained with synchrotron radiation (B), mammography (C), and conventional radiography (D) of a pregnant mouse at E18. Ossified fetal ribs stained red were observed (arrow), and ribs were visualized by synchrotron radiation with high resolution (arrowhead). Fetuses (white arrows) were identified by mammography and conventional radiograph; however, the fetuses were too small to identify anatomic structures.

bony structures were better defined at E18 and the skull, ribs, vertebrae, and extremities were identified. However, images of fetal bony structures from the mammography equipment were less resolved compared to those produced by synchrotron radiation (Figs. 4B and 5B).

Double-staining the fetal mice with Alcian blue and Alizarin red S showed that rib were not identifiable at E14 although a lack of staining does not necessarily indicate a lack of rib formation (Fig. 4A). However, calcified ribs and thoracic vertebrae were stained red at E18 (Fig. 5A). Ossified metatarsus, tibia, fibula, pelvis, scapula, humerus, ulna, radius, and skull were also observed at this stage in the double-stained fetal mice (Fig. 6). Synchrotron radiation imaging of the fetus removed from the uterus at E18 showed the ossified bony structures similar to the ones observed by double-staining an age-matched mouse fetus (Fig. 6).

Discussion

In this study, the mouse fetal skeleton was first visualized in a pregnant mouse by synchrotron radiation at E14. This was a day earlier than first visualization by mammography equipment (E15) and conventional radiography (E18). Fetal ribs appeared faintly on images of three out of the four mice examined with synchrotron radiation at E14. However, these images were not sufficient for examining the whole fetal skeleton. This was probably due to minimal calcification of the skeleton at this time point as observed in double-stained mouse fetuses. Although images of fetal skeletons visualized by the mammography equipment demonstrated that this modality is sufficient for examining the whole mouse skeleton, mammography might not be suitable for visualizing small bony structures due to the small size of fetus. At E18, fetal skeletons were more apparent and various bony structures such as ribs and vertebrae were visualized by synchrotron radiation with high magnification and resolution. However, since the field of view for synchrotron radiation was small (2 × 3 mm), it was difficult to define the anatomy of overlapping fetuses located in the uterus.

For the data acquisition, we can use a highly collimated and bright X-ray beam associated with refractive edge enhanced contrast and requiring a short exposure time. This enables us to obtain images of excellent quality with high resolution and video-rate acquisition. When transiting the sample, the beam obtains information on sample image contrast through two mechanisms: the attenuation coefficient and/or the path difference by refraction and/or diffraction. However, the density of a biological sample is too low to produce sufficient contrast. Therefore, the refractive edge enhanced contrast mechanism is dominant. Image information is obtained by the edge of an object having a different refractive index, which X-ray beam transmits to the scintillator, is partially converted into visible light, magnified by optical lens, and

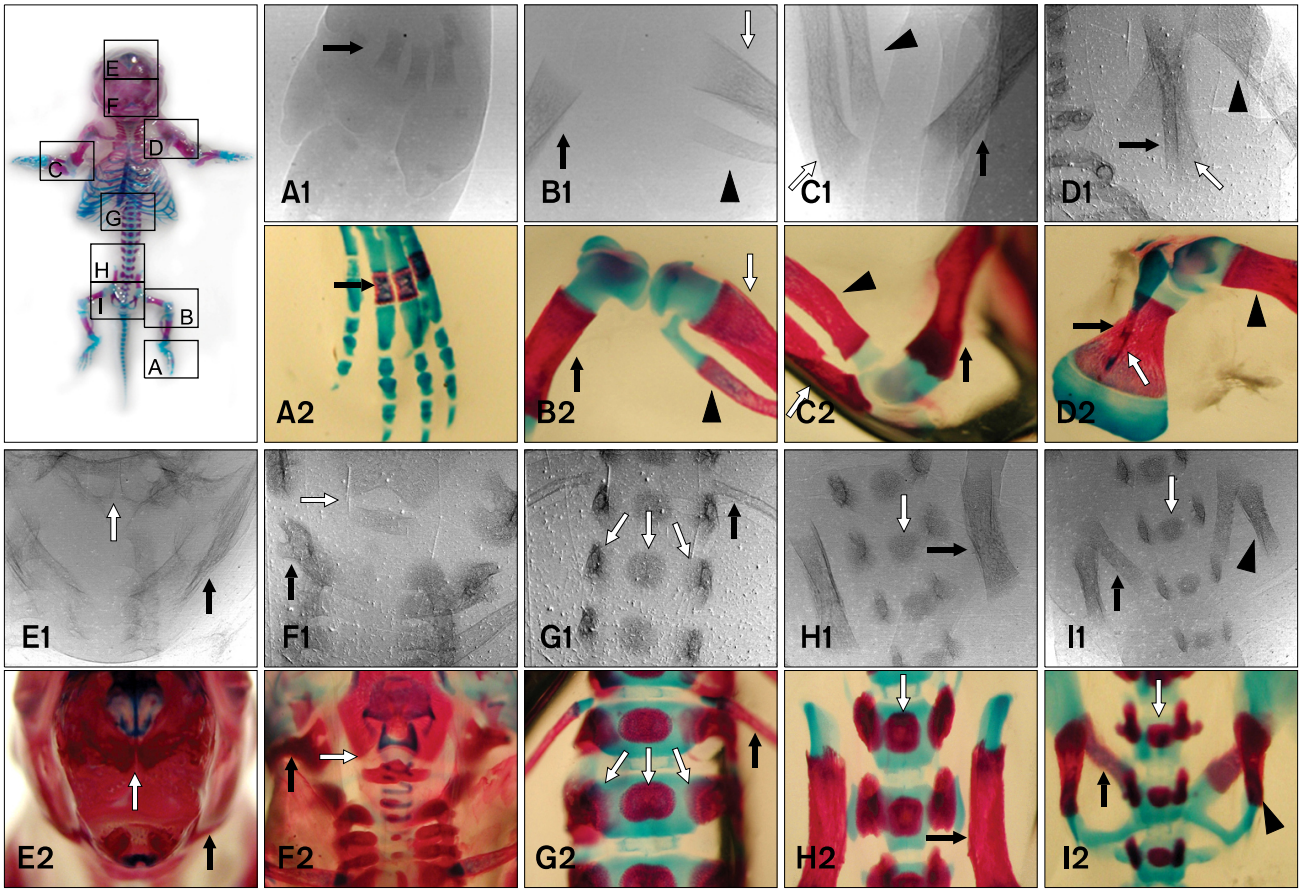

Fig. 6. Photographs of a fetus removed from a pregnant mouse at E18. The fetus was stained with Alizarin red S and Alcian blue. It was about 18 mm in length from crown to rump. Rectangles represent the field of views imaged by synchrotron radiation. A-I: comparisons of synchrotron radiation (1) and double-staining (2) images of the fetal mouse at E18, A: The fetal metatarsus showed calcified metatarsal bones (arrow), B: Distal femur (arrow), proximal tibia (white arrow), and fibula (arrowhead), C: Distal humerus (arrow), proximal radius (arrowhead), and ulna (white arrow), D: Scapula (arrow), proximal humerus (arrowhead), and spinous process of the scapula (white arrow), E: Mandible (arrow) and nasal bone (white arrow), F: Atlas (arrow) and foramen magnum (white arrow), G: Last rib (arrow) and first lumbar vertebra (white arrows), H: Body of ilium (arrow), sacrum (white arrow), I: Pubis (arrow), sacrum (white arrow) and ischium (arrowhead).

transferred to a computer by the CCD video camera. In our experiment, we set a mirror between the scintillator and optic lens and therefore used a reflective mode rather than a transmission mode. Thus, we intended to minimize the damage of the optic lens by receiving only visible light by selectively excluding X-rays [5-7].

X-rays and double-staining techniques have been used as important tools for laboratory animal research. These imaging systems permit researchers to screen animal models for mutations or pathologies, and to monitor disease progression and response to therapy [22,23]. For example, carbon monoxide has been shown to be teratogenic in mice using mammography, and an animal model of lumbosacral agenesis was non-invasively studied with radiography [12, 28]. Double-stained mouse fetus was also used for studying the influence of the p53 tumor suppressor gene on mouse skeletal development [1,20]. However, double-staining fetal tissue requires the sacrifice of laboratory animals. Therefore, it is impossible to observe sequential development (or ontogeny within a single organism) of the fetus with this technique. Additionally, the size of a typical mouse fetus is about 18～20 mm from crown to rump. This small size makes it impossible to observe small lesions in these structures using traditional X-ray-based techniques such as mammography. Also, micro-CT is a non-invasive method and useful tool for assessing skeletal microstructures [4]. The advantages of micro-CT include the ability to quantify soft tissues, generate 3D images, decrease the time for cesarean section or any staining, reduce waste production associated with staining, and potentially evaluate multiple stages of skeletal changes [18,27]. However, the micro-CT system has a number of limitations associated with spatial resolution required for examining an individual fetus and grayscale resolution for detecting adjacent objects with similar densities [26].

Synchrotron radiation is suitable for acquiring high quality

real-time images. This system can be exploited to generate micron-level properties of blood vessel in real-time without the use of contrast agents [8]. Because the projection of synchrotron radiation should be vertical to the object, the mouse being examined had to be positioned in an upright posture. Thus, the fetuses were displaced to the lower abdomen and overlapped each other. Consequently, this interfered with identifying fetal anatomic structures. Therefore, one mouse was sacrificed on E18 and the litter was examined with synchrotron radiation to observed mouse fetal anatomy initially depicted by synchrotron radiation. Synchrotron radiation imaging of the fetus that was removed from the uterus at E18 showed ossified bony structures. This finding was consistent with the results from double-staining the mouse fetuses. Although synchrotron radiation enabled visualization of the mouse fetal skeleton at E18 with high resolution, a greater beam size is desirable for imaging integrated bony structures of the mouse fetus such as the vertebral column, skull, and extremities. The main purpose of this study was to evaluate the use of synchrotron radiation as a means of detecting fine bony structures. The usefulness of this technique was determined by visualizing fetal mice skeleton and estimating the time when the fetal skeleton could be observed. Results from the present study show that synchrotron radiation enables the visualization of mouse fetal skeleton with sufficient image definition at E18.

In conclusion, synchrotron radiation systems are expected to be an effective tool for real-time visualization of micro-sized fine bony structures with high magnification. This technique could be used to make these observations at earlier gestation stages compared to other conventional methods. Synchrotron radiation may be a powerful tool for identifying for mutations or pathologies in mouse fetal skeletons as well as monitoring disease progression and response to therapy.

Acknowledgments

This work was supported by the grants of Korea Genetically Engineered Mouse Center Program through the National Research Foundation of Korea founded by the Ministry of Education, Science and Technology (20100020878) to Prof. Seong JK.

References

1. **Baatout S, Jacquet P, Michaux A, Buset J, Vankerkom J, Derradji H, Yan J, von Suchodoletz H, de Saint-Georges L, Desaintes C, Mergeay M.** Developmental abnormalities induced by X-irradiation in p53 deficient mice. In Vivo 2002, **16**, 215-221.
2. **Bailey LJ, Johnston MC, Billet J.** Effects of carbon monoxide and hypoxia on cleft lip in A/J mice. Cleft Palate Craniofac J 1995, **32**, 14-19.
3. **Farley FA, Hall J, Goldstein SA.** Characteristics of congenital scoliosis in a mouse model. J Pediatr Orthop 2006, **26**, 341-346.
4. **Guldberg RE, Lin ASP, Coleman R, Robertson G, Duvall C.** Microcomputed tomography imaging of skeletal development and growth. Birth Defects Res C Embryo Today 2004, **72**, 250-259.
5. **Hwu Y, Hsieh HH, Lu MJ, Tsai WL, Lin HM, Goh WC, Lai B, Je JH, Kim CK, Noh DY.** Coherence-enhanced synchrotron radiology: Refraction versus diffraction mechanisms. J Appl Phys 1999, **86**, 4613-4618.
6. **Hwu Y, Lai B, Mancini DC, Je JH, Noh DY, Bertolo M, Tromba G, Margaritondo G.** Coherence based contrast enhancement in x-ray radiography with a photoelectron microscope. Appl Phys Lett 1999, **75**, 2377-2379.
7. **Hwu Y, Tsai WL, Lai B, Mancini DC, Je JH, Noh DY, Youn HS, Hwang CS, Cerrina F, Swiech W, Bertolo M, Tromba G, Margaritondo G.** Use of photoelectron microscopes as X-ray detectors for imaging and other applications. Nucl Instrum Methods Phys Res A 1999, **437**, 516-520.
8. **Hwu Y, Tsai WL, Je JH, Seol SK, Kim B, Groso A, Margaritondo G, Lee KH, Seong JK.** Synchrotron microangiography with no contrast agent. Phys Med Biol 2004, **49**, 501-508.
9. **Itai Y, Takeda T.** Application of synchrotron radiation to medicine. Two-dimensional intravenous coronary arteriography and monochromatic x-ray computed tomography. Invest Radiol 1993, **28** (Suppl 3), S158-159.
10. **Lee KH, Hwu YK, Je JH, Tsai WL, Choi EW, Kim YC, Kim HJ, Seong JK, Yi SW, Ryo HS, Margaritondo G.** Synchrotron radiation imaging of internal structures in live animals. Yonsei Med J 2002, **43**, 25-30.
11. **Lewis R.** Medical applications of synchrotron radiation x-rays. Phys Med Biol 1997, **42**, 1213-1243.
12. **Loder RT, Hernandez MJ, Lerner AL, Winebrener DJ, Goldstein SA, Hensinger RN, Liu CY, Schork MA.** The induction of congenital spinal deformities in mice by maternal carbon monoxide exposure. J Pediatr Orthop 2000, **20**, 662-666.
13. **Meuli R, Hwu Y, Je JH, Margaritondo G.** Synchrotron radiation in radiology: radiology techniques based on synchrotron sources. Eur Radiol 2004, **14**, 1550-1560.
14. **Momose A, Takeda T, Itai Y.** Blood vessels: depiction at phase-contrast X-ray imaging without contrast agents in the mouse and rat–feasibility study. Radiology 2000, **217**, 593-596.
15. **Mori H, Hyodo K, Tobita K, Chujo M, Shinozaki Y, Sugishita Y, Ando M.** Visualization of penetrating transmural arteries *in situ* by monochromatic synchrotron radiation. Circulation 1994, **89**, 863-871.
16. **Murray FJ, Schwetz BA, Crawford AA, Henck JW, Quast JF, Staples RE.** Embryotoxicity of inhaled sulfur dioxide and carbon monoxide in mice and rabbits. J Environ Sci Health C 1979, **13**, 233-250.
17. **Neggers YH, Singh J.** Zinc supplementation to protein-deficient diet in CO-exposed mice decreased fetal mortality and malformation. Biol Trace Elem Res 2006, **114**, 269-279.
18. **Oest ME, Jones JC, Hatfield C, Prater MR.** Micro-CT evaluation of murine fetal skeletal development yields greater morphometric precision over traditional clear-staining methods. Birth Defects Res B Dev Reprod Toxicol 2008, **83**,

582-589.
19. **Ohtsuka S, Sugishita Y, Takeda T, Itai Y, Hyodo K, Ando M.** Dynamic intravenous coronary arteriography using synchrotron radiation and its application to the measurement of coronary blood flow. Jpn Circ J 1997, **61**, 432-440.
20. **Ohyama K, Chung CH, Chen E, Gibson CW, Misof K, Fratzl P, Shapiro IM.** p53 influences mice skeletal development. J Craniofac Genet Dev Biol 1997, **17**, 161-171.
21. **Schültke E, Fiedler S, Nemoz C, Ogieglo L, Kelly ME, Crawford P, Esteve F, Brochard T, Renier M, Requardt H, Le Duc G, Juurlink B, Meguro K.** Synchrotron-based intra-venous K-edge digital subtraction angiography in a pig model: A feasibility study. Eur J Radiol 2010, **73**, 677-681.
22. **Schwetz BA, Smith FA, Leong BKJ, Staples RE.** Teratogenic potential of inhaled carbon monoxide in mice and rabbits. Teratology 1979, **19**, 385-392.
23. **Singh J, Aggison L Jr, Moore-Cheatum L.** Teratogenicity and developmental toxicity of carbon monoxide in protein-deficient mice. Teratology 1993, **48**, 149-159.
24. **Suortti P, Thomlinson W.** Medical applications of synchrotron radiation. Phys Med Biol 2003, **48**, R1-35.
25. **Tanaka E, Tanaka A, Sekka T, Shinozaki Y, Hyodo K, Umetani K, Mori H.** Digitized cerebral synchrotron radiation angiography: quantitative evaluation of the canine circle of Willis and its large and small branches. AJNR Am J Neuroradiol 1999, **20**, 801-806.
26. **Wise LD, Winkelmann CT.** Micro-computed tomography and alizarin red evaluations of boric acid-induced fetal skeletal changes in Sprague-Dawley rats. Birth Defects Res B Dev Reprod Toxicol 2009, **86**, 214-219.
27. **Wise LD, Winkelmann CT.** Evaluation of hydroxyurea-induced fetal skeletal changes in Dutch belted rabbits by micro-computed tomography and alizarin red staining. Birth Defects Res B Dev Reprod Toxicol 2009, **86**, 220-226.
28. **Zimmerman EF, Scott WJ Jr, Collins MD.** Ethanol-induced limb defects in mice: effect of strain and Ro15-4513. Teratology 1990, **41**, 453-462.